

Strong-field ionization of diatomic molecules and companion atoms: Strong-field approximation and tunneling theory including nuclear motion

Thomas Kim Kjeldsen and Lars Bojer Madsen

Department of Physics and Astronomy, University of Aarhus, 8000 Århus C, Denmark

(Received 25 November 2004; published 24 February 2005)

We present a detailed comparison of strong-field ionization of diatomic molecules and their companion atoms with nearly equal ionization potentials. We perform calculations in the length and velocity gauge formulations of the molecular strong-field approximation and with the molecular tunneling theory, and in both cases we consider effects of nuclear motion. A comparison of our results with experimental data shows that the length gauge strong-field approximation gives the most reliable predictions.

DOI: 10.1103/PhysRevA.71.023411

PACS number(s): 33.80.Rv, 32.80.Rm

I. INTRODUCTION

When a molecule is subject to an intense laser field, a series of related strong-field processes may occur, including ionization, dissociation, and high-harmonic generation. As for atoms, it is essential to obtain a detailed understanding of the initial, single-ionization process in order to describe the subsequent evolution of the system. Fully *ab initio* calculations of the strong-field ionization of any molecule more complicated than H_2 are impossible in the foreseeable future. Hence, theories of general practical use have to rely on theoretical modeling and it is the purpose of the present work to investigate the accuracy of such models. While the quality of *ab initio* calculations may be checked numerically by studies of convergence and by identity of results in different gauges, the quality of an approximate model has to be checked against a more accurate model or experimental data.

In the study of strong-field ionization of molecules, three models are widely used. These are the velocity gauge (VG) molecular strong-field approximation (MO-SFA VG) [1], the length gauge (LG) MO-SFA (MO-SFA LG) [2], and the molecular tunneling theory [3]. The latter theory is an extension of the atomic Ammosov-Delone-Krainov (ADK) tunneling theory [4] generalized to take into account the nonspherical symmetry of the molecular system and it is referred to as the MO-ADK theory. The MO-SFA VG and MO-SFA LG theories are the velocity gauge and length gauge versions of the Keldysh-Faisal-Reiss (KFR) atomic theories [5–7] appropriately modified to the molecular case. In short, the MO-SFA theories are based on an *S*-matrix formulation where one considers the transition from a field-free initial state to a Volkov final state, i.e., the state of a free electron in the laser field.

To assess the quality of the models, predictions have been compared with experimental data (see, e.g., Ref. [3] and references therein). In particular, data has been studied in detail which compares ionization yields of diatomic molecules with yields of atoms having nearly the same electronic binding as the molecules—the so-called companion atoms. The ratio of ion signal data of diatomic molecules and their companion atoms [8–13] is illuminating since effects are factored out which depend only on the binding energy. Hence a comparison of the ratio of ionization signal of, e.g., N_2 and its com-

panion Ar atom allows one to study fairly directly effects of molecular symmetry and ro-vibrational motion. In Ref. [3] the status of theory versus experiments was discussed: The MO-ADK theory [3] gave results in satisfactory agreement with experiments for molecules with suppressed ionization, $D_2:Ar$ [10,13] and $O_2:Xe$ [8,11], and without, $N_2:Ar$ [11].

For the $F_2:Ar$ ratio, the MO-ADK theory predicts suppression of the molecular signal while the experimental data [12] does not. For the F_2 molecule, however, the total energy obtained from a Hartree-Fock (HF) calculation of the molecular system is higher than the energy of the separated atoms [14]. This means that electron correlation effects are important for the proper description of the binding of F_2 , and, accordingly, the one-electron model taken as the starting point for the MO-ADK (and the MO-SFA) theory is not applicable. The models discussed above, and in the present paper, can only be meaningfully applied on molecular systems where effects of electron-electron correlation are small [15]. Methods which do take electron-electron correlation into account are presently under development [16,17], but these methods are not yet applicable to molecules interacting with oscillating fields in geometries without cylindrical symmetry.

The MO-SFA VG was compared with experiments in Ref. [1]. The theory was shown to predict suppressed ionization of $O_2:Xe$ [8,11] and to predict the “absence” of suppressed ionization in $N_2:Ar$ [11]. In Ref. [18], the predictions of the MO-SFA VG were compared with experimental above-threshold-ionization spectra of O_2 (π_g symmetry) and N_2 (σ_g symmetry) and for these systems the theory gave the correct qualitative predictions.

In general, the MO-SFA VG approximation predicts suppressed ionization for diatomic molecules with an antibonding highest occupied molecular orbital (HOMO) and it predicts no suppression of the ionization of diatoms with a bonding HOMO. These general predictions are based on an analysis of the MO-SFA VG rate in terms of linear combinations of atomic orbitals where the antibonding (bonding) rate is proportional to $\sin^2(\mathbf{q}\cdot\mathbf{R}/2)$ [$\cos^2(\mathbf{q}\cdot\mathbf{R}/2)$] and $\mathbf{q}\cdot\mathbf{R}\ll 1$ where \mathbf{q} is the momentum of the outgoing electron and \mathbf{R} is the internuclear coordinate. For example, the MO-SFA VG approximation predicts suppressed ionization for O_2 with a HOMO of π_g symmetry and no suppression of the $D_2:Ar$

signal. This latter prediction is in contrast with experimental observation [13] and MO-ADK theory [3], and we shall return to this discrepancy below.

In view of the above discussion at least two questions need to be investigated in more detail. First, what is the quantitative prediction of the MO-SFA in the D_2 :Ar case? Second, is it possible to carry out a calculation in a more accurate approximation which sheds some light on the discrepancy between the MO-ADK calculations of Ref. [3] and the experimental results of Ref. [13]? To address related questions we have recently developed the necessary tools for computations in the velocity and length gauge formulations of the MO-SFA, and in addition we have set up a program for the evaluation of the molecular tunneling theory [2,15]. Our LG and VG versions of the MO-SFA are generalizations of the atomic adiabatic theory [19]. Our formulation of the MO-ADK theory follows Ref. [3], but our method of extracting the angular coefficients of relevance for the evaluation of the rate is different [2,15]. In this work, we extend our previous analysis, by taking effects of nuclear motion explicitly into account, and we show that the inclusion of nuclear vibrations may lead to a significantly lower rate. For the molecules considered in this paper nuclear motion is of significant importance for D_2 and NO while it leads to small effects in the final results for the other molecules studied.

The paper is organized as follows. In Sec. II, we describe the theories and provide a qualitative discussion of the effects of nuclear motion. In Sec. III, we give some calculational details; in Sec. IV we present the results of our calculations; and in Sec. V we conclude.

II. THEORY

In this section we describe the MO-SFA and MO-ADK theories and discuss how to account for effects of nuclear motion. In the MO-SFA one considers a state to state transition where the molecular states are generated from moving nuclei. On the contrary, in the MO-ADK there is no detailed specification of the final state in the strong-field ionization process, and in order to maintain a quasistatic tunneling picture one must fix the nuclei at an internuclear distance R and let the electron move in the R -dependent potential.

A. Molecular strong-field approximation including nuclear motion in the Born-Oppenheimer approximation

In the Coulomb gauge and in the dipole approximation the linearly polarized laser field may be described by the vector potential $\mathbf{A}(t)=\mathbf{A}_0 \cos \omega t$, where ω is the angular frequency. The corresponding electric field is obtained as $\mathbf{F}(t)=-\partial_t \mathbf{A}(t)$, i.e., $\mathbf{F}(t)=\mathbf{F}_0 \sin \omega t$. The interaction between the field and an N -electron system is [atomic units ($\hbar=m_e=e=a_0=1$) are used throughout]

$$V^{(\text{VG})}(t)=\sum_{j=1}^N \mathbf{A}(t) \cdot \mathbf{p}_j + \frac{\mathbf{A}^2(t)}{2}, \quad (1)$$

in the velocity gauge and

$$V^{(\text{LG})}(t)=\sum_{j=1}^N \mathbf{r}_j \cdot \mathbf{F}(t), \quad (2)$$

in the length gauge. In either gauge, we express the angular differential $dW/d\hat{\mathbf{q}}$ and total W rates as sums over n -photon absorptions [19]

$$\frac{dW}{d\hat{\mathbf{q}}} = 2\pi \sum_{n=n_0}^{\infty} |A_{qn}|^2 q_n, \quad (3)$$

$$W = 2\pi \sum_{n=n_0}^{\infty} \int |A_{qn}|^2 q_n d\hat{\mathbf{q}}, \quad (4)$$

where the transition amplitudes corresponding to the interaction $V^{(c)}(t)$ ($c=\{\text{VG, LG}\}$),

$$A_{qn}^{(c)} = \frac{1}{T} \int_0^T \langle \Psi_f | V^{(c)}(t) | \Psi_i \rangle dt, \quad (5)$$

involves integration over one period of the field $T=2\pi/\omega$, and $\langle \langle \rangle \rangle$ designates integration over both the electronic and nuclear coordinates. Here Ψ_i describes the molecular initial state and Ψ_f is the final state describing the state of the residual ion and the free electron in the laser field. In Eqs. (3) and (4), n_0 is the minimum number of photons needed to reach the continuum, and the momentum q_n is given by energy conservation. In the Born-Oppenheimer (BO) approximation q_n is determined by Eq. (10) below.

In the SFA we approximate the initial state by a field-free molecular state. In the BO approximation this state is a product of an electronic state and a ro-vibrational state labelled by ν_i, J_i . The electronic and vibrational states are typically the respective ground states. The rotational periods of the diatomic molecules are much longer than typical experimental pulse durations and therefore the rotational degrees of freedom may be neglected. The total energy of the initial state is

$$E_i = E_i^e(R_0) + E_{\nu_i}, \quad (6)$$

where $E_i^e(R_0)$ is the electronic eigenenergy at the internuclear equilibrium distance R_0 and E_{ν_i} is the vibrational eigenenergy of the nuclear Hamiltonian. If we approximate the electronic part of the initial wave function by the single-determinant HF wave function, the corresponding initial molecular wave function is

$$\Psi_i = \frac{1}{\sqrt{N!}} \det |\psi_1(\mathbf{r}_1) \psi_2(\mathbf{r}_2) \cdots \psi_N(\mathbf{r}_N)|_{R_0} \times \chi_{\nu_i}(R) e^{-iE_i t}, \quad (7)$$

where $\chi_{\nu_i}(R)$ is the initial vibrational wave function and the ψ_j 's are orthogonal single-electron wave functions. The electronic wave function is evaluated at the nuclear equilibrium distance R_0 since we assume, consistently with the BO picture, that it will be a slowly varying function of the internuclear distance. We have checked that the results are insensitive to this approximation.

We seek the transition amplitude to a single-electron Volkov state and a definite vibrational and electronic eigenstate of the molecular ion. The application of a Volkov wave in the final state means that the electron-ion interaction is neglected. Additionally, we assume that the electronic state of the ion is unrelaxed, i.e., only the HOMO is affected. The final state is then

$$\Psi_f = \frac{1}{\sqrt{N!}} \det|\psi_1(\mathbf{r}_1)\psi_2(\mathbf{r}_2)\cdots\psi_V(\mathbf{r}_N,t)|_{R_0} \times \chi_{v_f}^+(R) e^{-iE_f^+ t}, \quad (8)$$

where ψ_V is a $(2\pi)^{-3/2}$ normalized Volkov wave function and where the superscripts “+” denote the ionic state. The time-averaged energy of the electron in the laser field is $q_n^2/2 + U_p$, and the total final-state energy is

$$E_f = E_f^{e,+}(R_0) + E_{v_f}^+ + \frac{q_n^2}{2} + U_p, \quad (9)$$

where $U_p = F_0^2/4\omega^2$ is the ponderomotive potential, and where the final state momentum q_n is determined by energy conservation $n\omega = E_f - E_i$, i.e.,

$$q_n = \sqrt{2\{n\omega - [E_f^{e,+}(R_0) + E_{v_f}^+ - E_i^e(R_0) - E_{v_i}] - U_p\}}. \quad (10)$$

The transition amplitude of Eq. (5) can now be written as ($c = \{\text{VG, LG}\}$)

$$\begin{aligned} A_{qn}^{(c)} &= \frac{1}{T} \int_0^T \langle \chi_{v_f}^+(R) \psi_V(\mathbf{r}_N, t) | V_N^{(c)}(t) \\ &\times | \psi_N(\mathbf{r}_N; R_0) \chi_{v_i}(R) \rangle \exp[i(E_f^{e,+}(R_0) \\ &+ E_{v_f}^+ - E_i^e(R_0) - E_{v_i})t] dt, \end{aligned} \quad (11)$$

where the N -electron matrix element of the one-electron operators, Eqs. (1) and (2), has been simplified by the Slater-Condon rules [20] and where $V_N^{(c)}(t)$ is the transition operator for electron N . The integration over nuclear coordinates can be performed immediately to give

$$\begin{aligned} A_{qn}^{(c)} &= S_{v_f, v_i} \frac{1}{T} \int_0^T \int \psi_V^*(\mathbf{r}_N, t) V_N^{(c)}(t) \psi_N(\mathbf{r}_N; R_0) d\mathbf{r}_N \\ &\times e^{i[E_f^{e,+}(R_0) + E_{v_f}^+ - E_i^e(R_0) - E_{v_i}]t} dt, \end{aligned} \quad (12)$$

where S_{v_f, v_i} is the Franck-Condon (FC) factor

$$S_{v_f, v_i} = \int [\chi_{v_f}^+(R)]^* \chi_{v_i}(R) dR. \quad (13)$$

From Eq. (12), we find the following explicit expressions for the amplitudes

$$\begin{aligned} A_{qn}^{(\text{LG})} &= S_{v_f, v_i} \frac{1}{T} \int_0^T \left(-E_b - \frac{[\mathbf{q}_n + \mathbf{A}(t)]^2}{2} \right) \tilde{\psi}_N[\mathbf{q}_n + \mathbf{A}(t)] \\ &\times \exp i \left(n\omega t + \mathbf{q}_n \cdot \boldsymbol{\alpha}_0 \sin(\omega t) + \frac{U_p}{2\omega} \sin(2\omega t) \right) dt, \end{aligned} \quad (14)$$

$$\begin{aligned} A_{qn}^{(\text{VG})} &= S_{v_f, v_i} \left(-E_b - \frac{q_n^2}{2} \right) \tilde{\psi}_N(\mathbf{q}_n) \frac{1}{T} \int_0^T \exp i \left(n\omega t \right. \\ &\left. + \mathbf{q}_n \cdot \boldsymbol{\alpha}_0 \sin(\omega t) + \frac{U_p}{2\omega} \sin(2\omega t) \right) dt. \end{aligned} \quad (15)$$

In Eqs. (14) and (15), $\boldsymbol{\alpha}_0 = \mathbf{A}_0/\omega$ is the quiver radius, $\tilde{\psi}_N(\mathbf{q}) = (2\pi)^{-3/2} \int d\mathbf{r} e^{-i\mathbf{q}\cdot\mathbf{r}} \psi_N(\mathbf{r})$ is the momentum space wave function of the HOMO, and E_b is the energy difference between the final and initial state;

$$E_b = E_f^{e,+}(R_0) + E_{v_f}^+ - E_i^e(R_0) - E_{v_i}. \quad (16)$$

When we compare Eqs. (14) and (15), we see that the length gauge formulation accounts for a superimposed quiver motion in momentum space of the bound state electron via the presence of the $\mathbf{A}(t)$ term in the argument of the momentum space wave function. Such an effect is not present in the velocity gauge amplitude.

To account for the Coulomb interaction between the outgoing electron and the residual molecular ion one has typically introduced a Coulomb correction factor. In the velocity gauge, this factor is $C_{\text{Coul}}^{(\text{VG})} = (\kappa^3/F_0)^{2Z_{\text{ion}}/\kappa}$ with $\kappa = \sqrt{2E_b}$ [1] and Z_{ion} the charge of the residual ion, while in the length gauge $C_{\text{Coul}}^{(\text{LG})} = (2\kappa^3/F_0)^{2Z_{\text{ion}}/\kappa}$ [21]. Both correction factors were derived for the case of strong-field ionization of *atoms*, and hence do not take into account the molecular symmetry. In our evaluation of rates, we have found that much more precise results are obtained in the length gauge with $C_{\text{Coul}}^{(\text{LG})} = 1$ [2,15]. We explain the absence of a Coulomb interaction in the length gauge by the fact that the transition to the continuum occurs at large distances. In this spatial region the laser-electron interaction is stronger than the electron-ion interaction and the Volkov state is a good approximation for the final state. In addition to the Coulomb correction factor, we multiply the rates by the number of equivalent electrons in the HOMO. Finally, to obtain the total ionization rate of the molecules, we must sum the contributions from each vibrational level in the final state. In the velocity gauge our result is equivalent to that of Ref. [22]. For the noble gas atoms with filled p shells we sum the rates from each magnetic substate to obtain the total rate of ionization.

1. Qualitative discussion of the effect of nuclear motion

The transition amplitude of Eq. (12) consists of two factors, namely the Franck-Condon (FC) factor and an electronic matrix element, and both factors depend on the vibrational levels considered. The rates to each vibrational level are therefore not just proportional to the FC factors. Instead the relative populations in the lower final vibrational states are enhanced compared with the distribution obtained from the FC factors alone [22] because the electronic matrix element is favored by the smallest energy differences. When including vibrations, the total rate summed over all final vibrational states will therefore typically be smaller than if the vibrational ground state of the ion had been given the weight of unity. This latter method is nearly equivalent to fixing the nuclei {compare Eqs. (14) and (15) with Eqs. (5) and (6) of Ref. [2]}.

The importance of the inclusion of nuclear vibrations will depend on the properties of the neutral molecule and the molecular ion. If their potential curves are only shifted with respect to each other but otherwise exactly identical, then the vibrational eigenstates will be identical, too. The orthogonality of the nuclear wave functions then assures that only a single FC will be nonzero. We may estimate the importance of nuclear vibrations using molecular orbital theory and by considering the type of valence orbitals. If the valence orbital is nearly nonbonding as, e.g., in N_2 , the bonding properties of the molecular ion will be approximately equal to the bonding properties of neutral molecule and transitions between the vibrational ground states of the molecule and the ion dominate. In the case of a bonding HOMO, e.g., as in D_2 , the bonding of the ion will be weakened and transitions to many vibrational states will occur.

B. Molecular ADK theory

The tunneling theory [3,4] relies on the assumption that at any given instant of time the system will respond to the external laser field as if it were a static electric field. The rate of ionization in the oscillating field may then be determined by time-averaged static rates. Whether this approach is reasonable or not depends on the value of the Keldysh parameter $\gamma = \sqrt{2E_b}\omega/F_0$ [5] with $\gamma \ll 1$ in the tunneling regime. We will only show results from the MO-ADK theory in the intensity regions corresponding to $\gamma \leq 1$.

The tunneling rate of diatomic molecules can be determined once the field-free asymptotic wave function is known. In a body-fixed frame, labeled by superscript B and a z axis directed along the internuclear axis, this function has the asymptotic Coulomb form

$$\psi_N^B(\mathbf{r}) \sim r^{Z_{\text{ion}}/\kappa-1} e^{-\kappa r} \sum_l C_{lm} Y_{lm}(\hat{\mathbf{r}}), \quad (17)$$

where m is the projection of the angular momentum on the internuclear axis, and where C_{lm} are expansion coefficients.

From the asymptotic form of Eq. (17), the total ionization rate in a static (dc) field in the positive laboratory-fixed Z direction is calculated as in the atomic case [21,23,24], and the result is [3]

$$W_{\text{stat}}(F_0) = \sum_{m'} \frac{|B(m')|^2}{2^{|m'|} |m'|! \kappa^{2Z_{\text{ion}}/\kappa-1}} \times \left(\frac{2\kappa^3}{F_0} \right)^{2Z_{\text{ion}}/\kappa-|m'|-1} \exp\left(-\frac{2\kappa^3}{3F_0}\right), \quad (18)$$

where

$$B(m') = \sum_l (-1)^{(|m'|+m')/2} \sqrt{\frac{(2l+1)(l+|m'|)!}{2(l-|m'|)!}} \times C_{lm} d_{m'm}^{(l)}(\theta). \quad (19)$$

Here $d_{m'm}^{(l)}(\theta)$ is the middle term of Wigner's rotation function [25] and θ is the angle between the field direction and the internuclear axis.

In a slowly varying field, the ionization rate is found by averaging the dc rate over an optical cycle [15]

$$W \approx \sqrt{\frac{3F_0}{\pi\kappa^3}} \frac{W_{\text{stat}}^+(F_0) + W_{\text{stat}}^-(F_0)}{2}, \quad (20)$$

where $W_{\text{stat}}^\pm(F_0)$ are the dc rates for the positive and negative field directions with respect to the Z direction. When the field points in the negative Z direction, Eqs. (18) and (19) must be modified by the substitution $C_{lm} \rightarrow (-1)^l C_{lm}$ [15]. We see from Eqs. (18)–(20) that one only needs to know the C_{lm} coefficients in order to be able to evaluate the tunneling formula analytically. See also Ref. [15] for a generalization of the tunneling theory to molecules with more than two nuclei.

The tunneling theory can be extended to include effects of vibrations. In the quasistatic picture all potentials seen by the active electron should be regarded as being static. This means that the nuclei are fixed and the height of the tunneling barrier will depend on the internuclear distance chosen. We then calculate the rate for each value of R and weight these R -dependent rates by the R probability distribution obtained from the nuclear wave function [3]. As an approximate binding energy we take the energy difference between the potential curves of the ion and neutral molecule as calculated by HF theory. The vibrational wave functions are constructed from the harmonic approximation to experimental potential curves [26]. As demonstrated in Sec. IV the effect of this R -dependent weighting is quite small. Note in passing that recently vibrational distributions were measured and calculated with tunneling theory [27].

III. CALCULATIONAL DETAILS

In order to determine the angular coefficients C_{lm} we evaluate the ground state wave function in the HF approximation. We seek an accurate description of the orbitals at large distances with the correct exponential behavior. For this purpose we find in general the usual expansion in an atomic Gaussian basis to be inadequate. Instead we solve the HF equations fully numerically for the diatomic molecules [28] and for the atoms [29,30]. After having obtained the ground state orbitals we project the highest occupied orbital on the spherical harmonics and match the resulting radial functions to the form $C_{lm} r^{Z_{\text{ion}}/\kappa-1} e^{-\kappa r}$, treating the angular coefficients as fitting parameters. We give the C_{lm} 's obtained by this procedure in Table I. Since orbitals from the HF calculation are optimal within the independent particle approximation, the HF C_{lm} coefficients should be more accurate than the multiple scattering coefficients reported in Ref. [3].

The knowledge of the coefficients C_{lm} is sufficient to evaluate the MO-SFA LG rate accurately [15]. For the evaluation of the MO-SFA VG transition amplitudes, we make a numeric Fourier transform of the HOMO.

If we use the experimental ionization potential in the calculation of κ , the HOMO is not guaranteed to follow the correct asymptotic form of Eq. (17). The asymptotic form will be similar but with $\kappa^{\text{HF}} = \sqrt{2|\epsilon_{\text{HOMO}}^{\text{HF}}|}$ substituted for κ with ϵ_{HOMO} the eigenvalue of the one-electron HF

TABLE I. The molecular and atomic properties necessary for the evaluation of the present MO-SFA LG and the MO-ADK theory. I_p is the experimental adiabatic ionization potential and R_0 is the equilibrium distance [26]. Furthermore, we give the angular coefficients C_{lm} from our Hartree-Fock-based calculation together with the coefficients from Ref. [3]. We have chosen the origin at the geometrical midpoint. Franck-Condon factors and vibrational energies can be found in the references indicated after each molecular species.

		I_p (eV)	R_0 (Å)	C_{0m}	C_{1m}	C_{2m}	C_{3m}	C_{4m}	
$D_2 (\sigma_g)$	[32]	15.47	0.742	2.44		0.14		0.00	
				2.51		0.06		0.00	[3]
$N_2 (\sigma_g)$	[33]	15.58	1.098	3.46		1.64		0.12	
				2.02		0.78		0.04	[3]
$O_2 (\pi_g)$	[34]	12.03	1.208			1.04		0.07	
$S_2 (\pi_g)$	[35] ^a	9.36	1.889			0.62		0.03	[3]
						1.46		0.24	
CO (σ)	[34]	14.01	1.128	-3.93	2.79	-1.59	0.31	-0.09	
				1.43	0.76	0.28	0.02		[3]
NO (π)	[34]	9.26	1.151		-0.25	0.82	-0.06	0.04	
					0.22	0.41	0.01		[3]
SO (π)	[36] ^a	10.29	1.481		1.09	-1.25	0.34	-0.12	
					0.41	-0.31	0.01		[3]
Ar (p)		15.76			2.51				
					2.44				[3]
Kr (p)		14.00			2.59				
					2.49				[3]
Xe (p)		12.13			2.72				
					2.57				[3]

^aBased on photoelectron spectrum

(Roothaan) equation. For the highly correlated F^- ion, for example, the two different values of κ differ by 20% and the application of a wrong asymptotic wave function will introduce a large error when calculating the MO-SFA LG ionization rates [31]. For the systems considered here the largest difference between the experimental κ and κ^{HF} is 10% for NO and less than 5% for the remaining systems. Thus we conclude that correlation effects do not affect the outer electron significantly for the systems considered here. We believe that the smallness of the differences between κ and κ^{HF} justifies the application of the single-active electron models.

With the ionization rates at hand, we calculate the ion signals by integrating over the temporal and spatial profile of the pulse [15,37]. In all experiments discussed here, the ions were collected through a small pinhole near the beam waist and the spatial integration should be restricted to this region. As the signals saturate, the signal ratios will approach unity for such a setup. We calculate the rates and signals for each molecular orientation and average the signals over orientations in order to simulate randomly oriented ensembles.

IV. RESULTS AND DISCUSSION

A. $N_2:Ar$

Several experiments have been performed on N_2 and its companion atom Ar [9,11,12,18], and there are significant

disagreements between the results. The yield ratios were estimated to be $N_2:Ar \approx 0.7$ [11], 0.2 [9], 1 [18], and 1.7 [12], respectively. Previous theoretical calculations with the MO-SFA VG model predicted the $N_2:Ar$ ratio to be above unity [1] while MO-ADK calculations predicted the ratio to be 0.4–0.6. In Ref. [3] it was shown that the experimental differences could not be explained by differences in pulse lengths and the possibility of dynamical alignment.

In Fig. 1 we show our calculations for the $N_2:Ar$ ratio. First, we note that the results from each model are nearly independent of pulse duration. In the length gauge we predict the ion yields of N_2 and Ar to be nearly identical. These findings are in reasonable agreement with the experimental data from Refs. [11,12]. The differences between our MO-ADK results and the results of Ref. [3] lie in the values of the angular C_{lm} coefficients. We find the ratio to be slightly lower than unity in agreement with Ref. [11] [Fig. 1(a)]. The velocity gauge MO-SFA predicts the ion yield of N_2 to be somewhat larger than for Ar in accordance with Ref. [1]. We find an oscillating behavior of the signal ratio in the velocity gauge which is not supported by the experimental data. The origin of this artifact lies in the concept of channel closing: At low intensities continuum-continuum transitions are very weak. The rate of ionization is then typically dominated by the rate which originates from the lowest number of photon absorptions, n_0 . As the intensity increases the ponderomotive

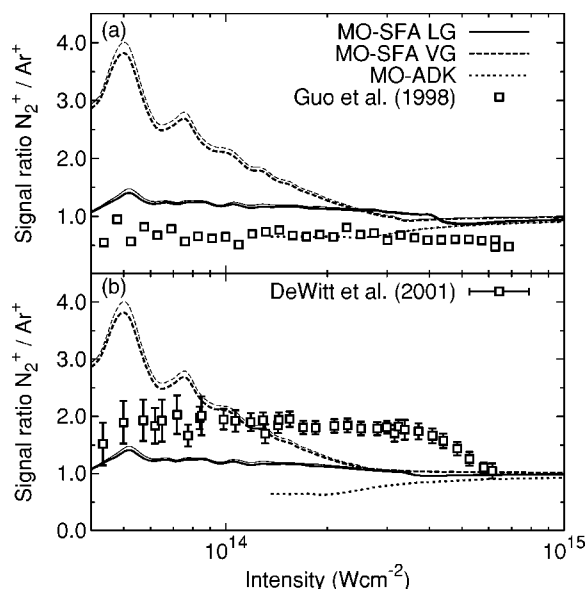


FIG. 1. Intensity-dependent ratios between the yields of N_2^+ and Ar ions. In both panels the laser wavelength is 800 nm. In panel (a), the pulse duration is 30 fs and the experimental data is from Ref. [11]. In panel (b), the pulse duration is 100 fs and the experimental data is from Ref. [12]. The thin lines are calculations with fixed nuclei and the thick lines are the corresponding calculations including vibrations.

potential rises and eventually leads to the closing of the n_0 channel. The effect of channel closing on the total ionization rate depends on the relative importance of the n_0 process compared with the excess-photon processes. As the intensity increases and a channel closing approaches, the momentum corresponding to n_0 photon absorptions will become small. If the HOMO does not contain an $l=0$ component, then $\tilde{\psi}_N \rightarrow 0$ as $q \rightarrow 0$, and for such systems the MO-SFA VG amplitude, Eq. (15), will be suppressed. Near the channel closings the contribution from the n_0 channel is thus small and the total rate will not be significantly affected when this channel closes. If, on the other hand, the HOMO contains an $l=0$ component, the low momenta will generally be favored and the n_0 channel gives a large contribution of the total rate. In this case, the closing of a channel will therefore lead to an abrupt decrease of the total rate. These differences were previously mentioned in Ref. [38]. In the length gauge, the n_0 channel will be important regardless of the type of orbital due to the presence of $A(t)$ in the argument of the momentum space wave function [see Eq. (15)] and we always find abrupt decreases of the rate across a channel closing. We show the various effects described above in Fig. 2. The HOMO of N_2 is a σ_g ($l=0$ component) orbital and correspondingly we find a local minimum in the rate around the channel closings. The highest occupied atomic orbitals of Ar are the degenerate p ($l=1$) orbitals, and we find local minima in the length gauge rate while the velocity gauge rate increases smoothly near the channel closings. The differences between the parallel and perpendicular geometries of N_2 in the two gauges were explained in Ref. [2].

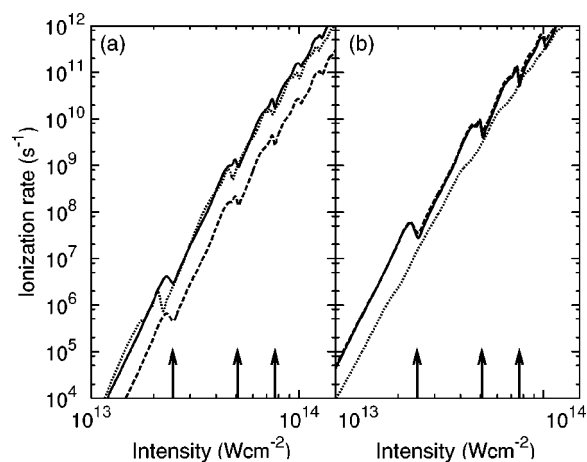


FIG. 2. The ionization rates of N_2 and Ar (dotted) at intensities around the first channel closings obtained from (a) MO-SFA LG and (b) MO-SFA VG. For N_2 , we give the rates at parallel (solid) and at perpendicular geometry (long-dashed). The wavelength is 800 nm and the intensities at which the channels close for N_2 are indicated by the arrows. Ar has a slightly higher ionization potential and the corresponding intensities lie at bit lower.

B. D_2 :Ar

Two experiments have been reported on D_2 and Ar [10,13] and both showed a suppression of the D_2 signal compared with the Ar signal. As mentioned in the Introduction the MO-ADK calculations reproduced this result [3] while the MO-SFA VG model predicts an absence of suppression because the HOMO of D_2 is a bonding σ_g orbital.

In Fig. 3, we show our calculations and the experimental sets of data. We do indeed find absence of suppressed ionization when we use the MO-SFA VG model. On the other hand, the MO-SFA LG and MO-ADK models both correctly predict suppression. At high intensities the ratio will approach unity as both signals saturate. The MO-SFA LG model has some problems in predicting the correct intensity at which this saturation occurs, but we note that the experiments do not agree on the saturation intensity either. The longer pulse length should be equivalent to a lower saturation intensity but this is clearly not the case when comparing the experimental data in Figs. 3(a) and 3(b).

We see that the inclusion of nuclear vibrations reduces the MO-SFA ratios by a significant factor compared with the fixed nuclei calculations. The origin of this effect was discussed in Sec. II A 1. The point is simply that the inclusion of vibrational motion will reduce the rate when the molecule and the molecular ion have different bonding properties and transitions to many different vibrational states occur.

C. O_2 :Xe

Suppressed ionization of O_2 :Xe has been observed repeatedly [8,11,12]. Theoretically, this was explained in the MO-SFA VG by the antibonding character of the π_g HOMO of O_2 [1]. Another explanation within the MO-ADK model was given in Ref. [3] where the interpretation was based on the asymptotic charge density of the π_g HOMO. At some

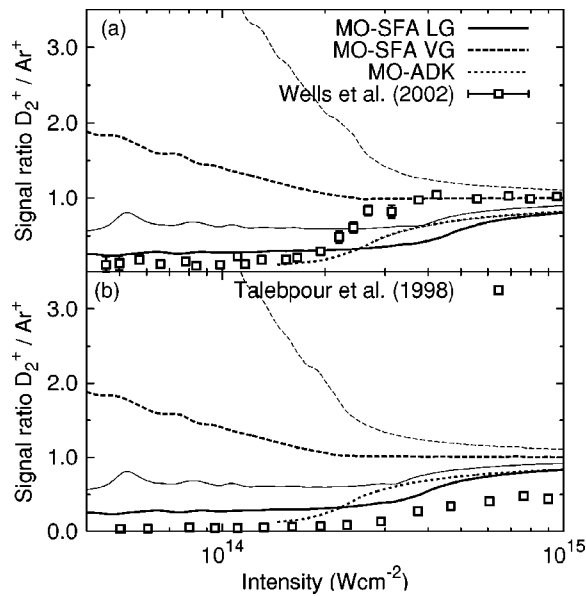


FIG. 3. Intensity-dependent ratios between the yields of D_2 and Ar ions. In both panels the laser wavelength is 800 nm. The thin lines are calculations with fixed nuclei and the thick lines are the corresponding calculations including vibrations. In panel (a), the pulse duration is 100 fs and the experimental data is from Ref. [13]. In panel (b), the pulse duration is 200 fs and the experimental data is from Ref. [10].

molecular orientations the electronic density will be preferentially perpendicular to the polarization axis and the rate of ionization will then be very small. Finally, in Ref. [39], it was proposed that nuclear dynamics could be responsible for the suppression. In Fig. 4, we show the experimental data together with our calculations. Clearly, all experiments and calculations show suppressed ionization of O_2 . Before saturation effects become important the theoretical MO-SFA VG predicts strongest suppression with the ratio below 0.01 while the ratio in MO-SFA LG is ≈ 0.03 . At low intensities, the experimental ratios are scattered between 0.02 and 0.20, which again makes a quantitative comparison with theories difficult. In the tunneling regime, beyond the intensity of $10^{14} \text{ W cm}^{-2}$, the MO-ADK model predicts that saturation effects are already important and thereby the degree of suppression is masked. Experimentally, saturation sets in at much higher intensities around $2 \times 10^{14} \text{ W cm}^{-2}$, in good agreement with the MO-SFA theories.

D. CO:Kr

The ion signal ratio of CO:Kr was measured in Ref. [13] and found to be around 1/2. In Figs. 5(a) and 5(b) we show the results at 800 and 1365 nm, respectively. Under the experimental conditions at 800 nm, the Keldysh parameter exceeds unity. Thus we cannot rely on the MO-ADK theory and in Fig. 5(a) we show only MO-SFA calculations. Both theories predict the ratio to be slightly larger than one. In the MO-SFA VG model, we find that the ratio depends on the intensity in a similar way as the N_2 :Ar ratio, and since the electronic structures of CO and Kr are nearly identical to N_2

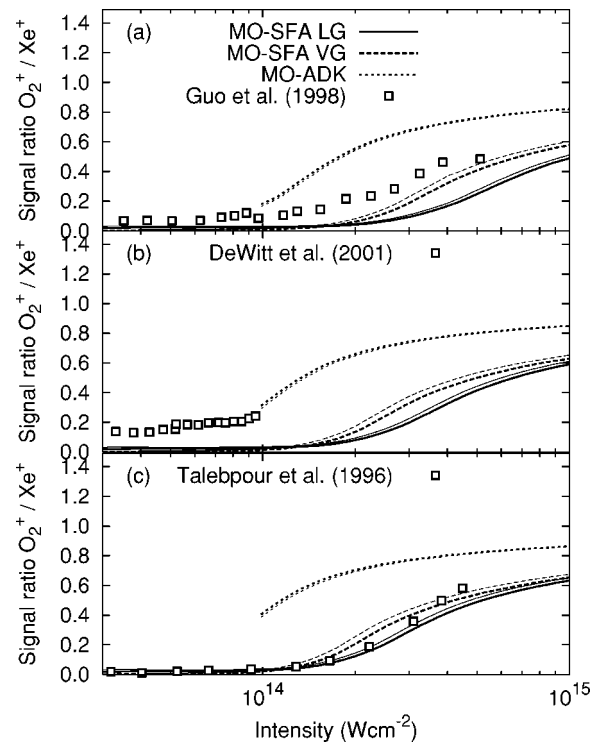


FIG. 4. Intensity-dependent ratios between the yields of O_2 and Xe ions. In all panels the laser wavelength is 800nm. The thin lines are calculations with fixed nuclei and the thick lines are the corresponding calculations including vibrations. In panel (a), the pulse duration is 30 fs and the experimental data is from Ref. [11]. In panel (b), the pulse duration is 100fs and the experimental data is from Ref. [12]. In panel (c) the pulse duration is 220 fs and the experimental data is from Ref. [8].

and Ar, respectively, we can explain the oscillating behavior by the same channel-closing argument (see Sec. IV A).

At 1365 nm and in the intensity range of Fig. 5(b), we would expect to be in the tunneling regime. Despite the fact that the tunneling theory should be applicable, the MO-ADK model predicts the ratio to be somewhat too large. Finally, we note that the result of our MO-ADK calculation is approximately an order of magnitude larger than the result from Ref. [3]. The only differences between these two calculations are the coefficients $C_{l,m=0}$ and the time-averaging of the static field rate, our Eq. (20) as compared with Eq. (10) of Ref. [3].

E. Molecules without companion atoms

In Ref. [13] the ion signal ratios of the pairs S_2 :Xe, NO:Xe, and SO:Xe were measured. Common to these pairs is that the ionization potential of Xe is somewhat higher than the ionization potentials of the molecules. The ratios measured are thus the results of both the structural differences (orientation, electronic wave functions) and the difference between the binding energies. The experiments were performed at the wavelength 800 nm with $\gamma > 1$, Fig. 6, and at 1365 nm with $\gamma < 1$, Fig. 7.

The electronic structure of S_2 is similar to O_2 and we should therefore expect the ionization of S_2 to be suppressed,

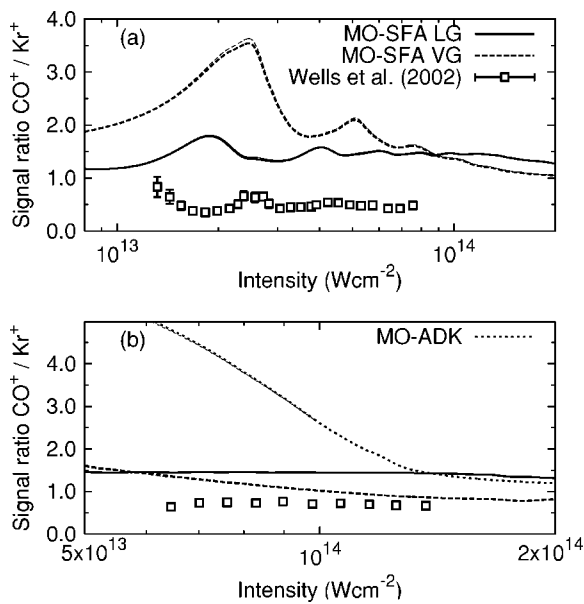


FIG. 5. Intensity-dependent ratios between the yields of CO and Kr ions. In panel (a) the laser wavelength is 800 nm and the pulse duration is 100 fs. In panel (b) the laser wavelength is 1365 nm and the pulse duration is 80 fs. In both panels the experimental data is from Ref. [13]. The thin lines are calculations with fixed nuclei and the thick lines are the corresponding calculations including vibrations.

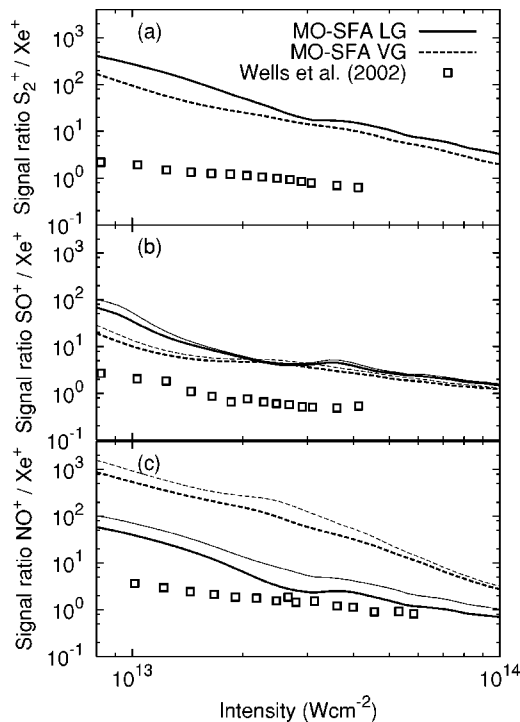


FIG. 6. Intensity-dependent ratios between the ion yields of (a) $S_2:Xe$, (b) $SO:Xe$, and (c) $NO:Xe$. In all panels the laser wavelength is 800 nm, the pulse duration is 100 fs, and the experimental data is from Ref. [13]. The thin lines are calculations with fixed nuclei and the thick lines are the corresponding calculations including vibrations.

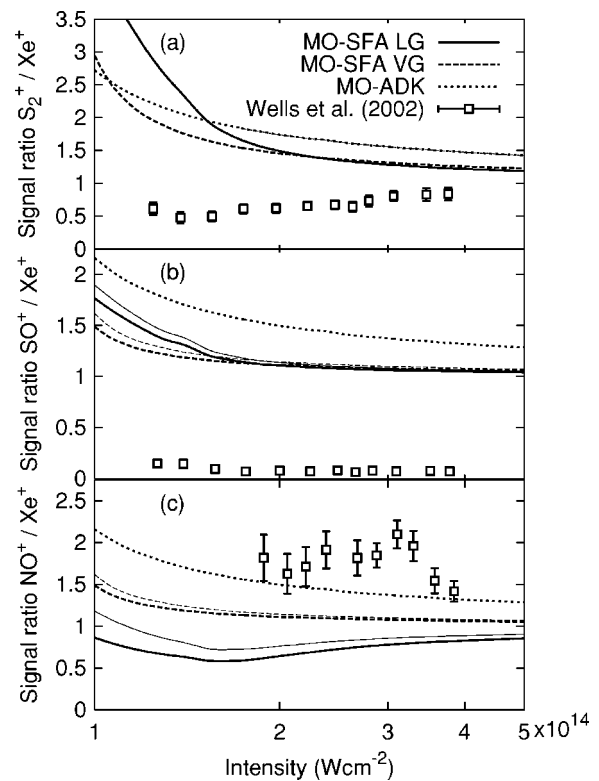


FIG. 7. Intensity-dependent ratios between the ion yields of (a) $S_2:Xe$, (b) $SO:Xe$, and (c) $NO:Xe$. In all panels the laser wavelength is 1365 nm, the pulse duration is 80 fs, and the experimental data is from Ref. [13]. The thin lines are calculations with fixed nuclei and the thick lines are the corresponding calculations including vibrations.

too. Our MO-SFA calculations, shown in Fig. 6(a), predict the $S_2:Xe$ ratio to be much higher than measured. Experimentally, the ratio was determined to be around unity. This indicates that ionization of S_2 would indeed be suppressed if compared with a hypothetical companion ion. In Figs. 6(b) and 6(c) we show the calculations for $SO:Xe$ and $NO:Xe$ and find a similar disagreement between theory and experiment for these pairs. The two previous attempts [3,13] to explain the ratios in this intensity regime overestimated the ratios by three to five orders of magnitude. Both calculations were based on tunneling models—in Ref. [13] a purely atomic ADK model was used and in Ref. [3] the MO-ADK model was applied. Our present MO-SFA calculations including nuclear motion are significantly closer to the experimental data but the agreement is still poor.

In Fig. 7 we show calculations and experimental data at the wavelength of 1365 nm, i.e., in the tunneling regime. The experiments were performed at such a high intensity that saturation effects become important in all our calculations and correspondingly, the ratios are all around unity. These predictions are in agreement with the experiment for $S_2:Xe$, Fig. 7(a), and $NO:Xe$, Fig. 7(c). From Fig. 7(b) we see that the $SO:Xe$ ratio is much lower than unity. This is quite remarkable since all three ratios in Fig. 6 were nearly identical at 800 nm but very different at 1365 nm—such wavelength dependencies are of course impossible to predict by quasi-static tunneling theories.

V. CONCLUSIONS

We have made a detailed study of strong-field ionization of diatomic molecules and their companion atoms. In particular we have investigated whether the approximate models, MO-SFA LG, MO-SFA VG and MO-ADK, are able to correctly predict the presence or absence of suppressed ionization in certain molecules. Furthermore, we have considered how nuclear vibrations can be taken into account within the adiabatic theory and the single-active electron approximation.

All models did correctly predict the absence of suppressed ionization for $N_2:Ar$ and the presence of suppressed ionization for $O_2:Xe$. Quantitative comparisons were made difficult due to disagreements between different experiments, and further experiments would therefore be highly desirable.

We find a rather good overall agreement between the MO-SFA LG theory and experiments on diatomic molecules and their companion atoms, and we believe that the MO-SFA LG model accounts quite well for the structural dependency on the strong-field ionization rates. In general we found the length gauge MO-SFA to be in better agreement with experiments than the velocity gauge MO-SFA—in particular in the case of $D_2:Ar$ where the MO-SFA VG predicted no suppression of ionization in contradiction with the experimental findings and the other theories.

The MO-ADK predictions were mostly in accordance with previously published results using this model [3]. For

the cases $N_2:Ar$, $D_2:Ar$, and $O_2:Xe$ these predictions are also in qualitative agreement with experimental data.

The most significant differences between the MO-ADK and the MO-SFA LG calculations are the much lower ratios predicted by the latter theory in the cases $O_2:Xe$ and $CO:Kr$. In both cases the results of the MO-SFA LG model agreed better with the experiments. This is interesting in view of recent experiments [40] which reported suppression of strong-field ionization for transition metal atoms relative to expectations, but only compared with tunneling theory, and not SFA. For the future work it would be interesting to check the SFA LG model on the transition metals to investigate if the suppression is due to a general breakdown of the single-active electron models or if it is due only to a failure of the ADK model.

All the models considered here fail to predict the correct ratio between molecules and atoms with different ionization potentials. This indicates that the dependency on the electronic binding energy is not correctly accounted for and points to the need for the development of improved models, including electron-electron correlations and exact final states.

ACKNOWLEDGMENTS

We would like to thank A. Saenz for useful discussions. L.B.M. is supported by the Danish Natural Science Research Council (Grant No. 21-03-0163).

-
- [1] J. Muth-Böhm, A. Becker, and F. H. M. Faisal, *Phys. Rev. Lett.* **85**, 2280 (2000).
- [2] T. K. Kjeldsen and L. B. Madsen, *J. Phys. B* **37**, 2033 (2004).
- [3] X. M. Tong, Z. X. Zhao, and C. D. Lin, *Phys. Rev. A* **66**, 033402 (2002).
- [4] M. V. Ammosov, N. B. Delone, and V. P. Krainov, *Sov. Phys. JETP* **64**, 1191 (1986).
- [5] L. V. Keldysh, *Sov. Phys. JETP* **20**, 1307 (1965).
- [6] F. H. M. Faisal, *J. Phys. B* **6**, L89 (1973).
- [7] H. R. Reiss, *Phys. Rev. A* **22**, 1786 (1980).
- [8] A. Talebpour, C. Y. Chien, and S. L. Chin, *J. Phys. B* **29**, L677 (1996).
- [9] Y. Liang, A. Talebpour, C. Y. Chien, and S. L. Chin, *J. Phys. B* **30**, 1369 (1997).
- [10] A. Talebpour, S. Larochelle, and S. L. Chin, *J. Phys. B* **31**, 2769 (1998).
- [11] C. Guo, M. Li, J. P. Nibarger, and G. N. Gibson, *Phys. Rev. A* **58**, R4271 (1998).
- [12] M. J. DeWitt, E. Wells, and R. R. Jones, *Phys. Rev. Lett.* **87**, 153001 (2001).
- [13] E. Wells, M. J. DeWitt, and R. R. Jones, *Phys. Rev. A* **66**, 013409 (2002).
- [14] T. Helgaker, P. Jørgensen, and J. Olsen, *Molecular Electronic-Structure Theory* (John Wiley & Sons, Chichester, 2000).
- [15] T. K. Kjeldsen, C. Z. Bisgaard, L. B. Madsen, and H. Stapelfeldt, *Phys. Rev. A* **71**, 013418 (2005).
- [16] X. Chu and S.-I. Chu, *Phys. Rev. A* **64**, 063404 (2001).
- [17] T. Otobe, K. Yabana, and J. I. Iwata, *Phys. Rev. A* **69**, 053404 (2004).
- [18] F. Grasbon *et al.*, *Phys. Rev. A* **63**, 041402(R) (2001).
- [19] G. F. Gribakin and M. Y. Kuchiev, *Phys. Rev. A* **55**, 3760 (1997).
- [20] E. U. Condon, *Phys. Rev.* **36**, 1121 (1930).
- [21] A. M. Perelomov, V. S. Popov, and M. V. Terent'ev, *Sov. Phys. JETP* **23**, 924 (1966).
- [22] A. Becker, A. D. Bandrauk, and S. L. Chin, *Chem. Phys. Lett.* **343**, 345 (2001).
- [23] B. M. Smirnov and M. I. Chibisov, *Sov. Phys. JETP* **22**, 585 (1966).
- [24] C. Z. Bisgaard and L. B. Madsen, *Am. J. Phys.* **72**, 249 (2004).
- [25] R. N. Zare, *Angular Momentum* (Wiley, New York, 1988).
- [26] *NIST Chemistry WebBook, NIST Standard Reference Database Number 69*, edited by P. J. Linstrom and W. G. Mallard (National Institute of Standards and Technology, Gaithersburg MD, 2003).
- [27] X. Urbain *et al.*, *Phys. Rev. Lett.* **92**, 163004 (2004).
- [28] J. Kobus, L. Laaksonen, and D. Sundholm, *Comput. Phys. Commun.* **98**, 346 (1996).
- [29] C. F. Fischer, *Comput. Phys. Commun.* **43**, 355 (1986).
- [30] G. Gaigalas and C. F. Fischer, *Comput. Phys. Commun.* **98**, 255 (1996).
- [31] G. F. Gribakin, V. K. Ivanov, A. V. Korol, and M. Y. Kuchiev, *J. Phys. B* **33**, 821 (2000).
- [32] G. H. Dunn, *J. Chem. Phys.* **44**, 2592 (1966).
- [33] M. Halmann and I. Laulicht, *J. Chem. Phys.* **43**, 1503 (1965).

- [34] R. Nicholls, *J. Phys. B* **1**, 1192 (1968).
- [35] J. Berkowitz, *J. Chem. Phys.* **62**, 4074 (1975).
- [36] J. Dyke *et al.*, *J. Chem. Phys.* **106**, 821 (1997).
- [37] B. Chang, P. R. Bolton, and D. N. Fittinghoff, *Phys. Rev. A* **47**, 4193 (1993).
- [38] A. Jaroń-Becker, A. Becker, and F. H. M. Faisal, *Phys. Rev. A* **69**, 023410 (2004).
- [39] A. Saenz, *J. Phys. B* **33**, 4365 (2000).
- [40] M. Smits, C. A. de Lange, A. Stolow, and D. M. Rayner, *Phys. Rev. Lett.* **93**, 213003 (2004).